$$T_{mn} = \frac{k_B T}{8\pi^3} q_m \int\int \left(\mathbf{A}^{-1}\right)_{mn} \mathrm{d}S,$$

where $q_m$ is the radius of the sphere that replaces the anisotropic region (Fig. 7.4.2.2) actually scanned in the experiment, and $\mathrm{d}S$ is a surface element of this sphere. $q_m$ can be estimated by equating the volume of the sphere to the volume swept out in the scan.

If *both* approximations are employed, the correction factor is isotropic and reduces to

$$\alpha = \frac{H^2 k_B T q_m}{3\pi^2 \rho \mathbf{v}_L^2}, \qquad (7.4.2.14)$$

with $\mathbf{v}_L$ representing the mean velocity of the elastic waves, averaged over all directions of propagation and of polarization.

Experimental values of $\alpha$ have been measured for several crystals by $\gamma$-ray diffraction of Mössbauer radiation (Krec & Steiner, 1984). In general, there is good agreement between these values and those calculated by the numerical methods, which take into account anisotropy of the TDS. The correction factors calculated analytically from (7.4.2.14) are less satisfactory.

The principal effect of *not* correcting for TDS is to underestimate the values of the atomic displacement parameters. Writing $\exp\alpha \approx 1 + \alpha$, we see from (7.4.2.14) that the overall displacement factor is increased from $B$ to $B + \Delta B$ when the correction is made. $\Delta B$ is given by

$$\Delta B = \frac{8 k_B T q_m}{3\pi^2 \rho \mathbf{v}_L^2}.$$

Typically, $\Delta B/B$ is 10–20%. Smaller errors occur in other parameters, but, for accurate studies of charge densities or bonding effects, a TDS correction of all integrated intensities is advisable (Helmholdt & Vos, 1977; Stevenson & Harada, 1983).

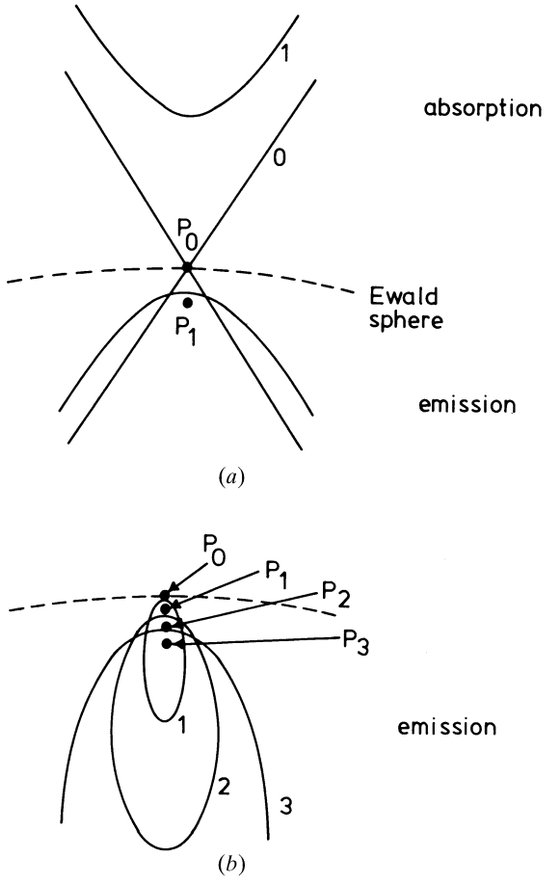


Fig. 7.4.2.3. Scattering surfaces for one-phonon scattering of neutrons: (*a*) for neutrons faster than sound ($\beta < 1$); (*b*) for neutrons slower than sound ($\beta > 1$). The scattering surface for X-rays is the Ewald sphere. $P_0$, $P_1$, *etc*. are different positions of the reciprocal-lattice point with respect to the Ewald sphere, and the scattering surfaces are numbered to correspond with the appropriate position of $P$.

### 7.4.2.3. *TDS correction factor for thermal neutrons (single crystals)*

The neutron treatment of the correction factor lies along similar lines to that for X-rays. The principal difference arises from the different topologies of the one-phonon 'scattering surfaces' for X-rays and neutrons. These surfaces represent the locus in reciprocal space of the end-points of the phonon wavevectors $\mathbf{q}$ (for fixed crystal orientation and fixed incident wavevector $\mathbf{k}_0$) when the wavevector $\mathbf{k}$ of the scattered radiation is allowed to vary. We shall not discuss the theory for pulsed neutrons, where the incident wavelength varies (see Popa & Willis, 1994).

The scattering surfaces are determined by the conservation laws for momentum transfer,

$$\mathbf{H} = \mathbf{k} - \mathbf{k}_0 = 2\pi\mathbf{h} + \mathbf{q},$$

and for energy transfer,

$$\hbar^2\left(k^2 - k_0^2\right)/2m_n = -\varepsilon\hbar\omega_j(\mathbf{q}), \qquad (7.4.2.15)$$

where $m_n$ is the neutron mass and $\hbar\omega_j(\mathbf{q})$ is the phonon energy. $\varepsilon$ is either $+1$ or $-1$, where $\varepsilon = +1$ corresponds to phonon emission (or phonon creation) in the crystal and a loss in energy of the neutrons after scattering, and $\varepsilon = -1$ corresponds to phonon absorption (or phonon annihilation) in the crystal and a gain in neutron energy. In the X-ray case, the phonon energy is negligible compared with the energy of the X-ray photon, so that (7.4.2.15) reduces to

$$k = k_0,$$

and the scattering surface is the Ewald sphere. For neutron scattering, $\hbar\omega_j(\mathbf{q})$ is comparable with the energy of a thermal neutron, and so the topology of the scattering surface is more complicated. For one-phonon scattering by long-wavelength acoustic modes with $q \ll k_0$, (7.4.2.15) reduces to

$$k = k_0 - \varepsilon\beta q,$$

where $\beta$ ($= \mathbf{v}_L/\mathbf{v}_n$) is the ratio of the sound velocity in the crystal and the neutron velocity. If the Ewald sphere in the neighbourhood of a reciprocal-lattice point is replaced by its tangent plane, the scattering surface becomes a conic section with eccentricity $1/\beta$. For $\beta < 1$, the conic section is a hyperboloid of two sheets with the reciprocal-lattice point $P$ at one focus. The phonon

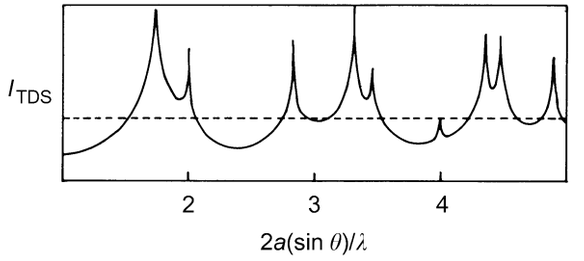


Fig. 7.4.2.4. One-phonon scattering calculated for polycrystalline nickel of lattice constant $a$ (after Suortti, 1980).

wavevectors on one sheet correspond to scattering with phonon emission and on the other sheet to phonon absorption. For $\beta > 1$, the conic section is an ellipsoid with $P$ at one focus. Scattering now occurs either by emission or by absorption, but not by both together (Fig. 7.4.2.3).

To evaluate the TDS correction, with **q** restricted to lie along the scattering surfaces, separate treatments are required for faster-than-sound ($\beta < 1$) and for slower-than-sound ($\beta > 1$) neutrons. The final results can be summarized as follows (Willis, 1970; Cooper, 1971):

(*a*) For faster-than-sound neutrons, the TDS rises to a maximum, just as for X-rays, and the correction factor is given by (7.4.2.13), which applies to the X-ray case. (This is a remarkable result in view of the marked difference in the one-phonon scattering surfaces for X-rays and neutrons.)

(*b*) For slower-than-sound neutrons, the correction factor depends on the velocity (wavelength) of the neutrons and is more difficult to evaluate than in (*a*). However, $\alpha$ will always be less than that calculated for X-rays of the same wavelength, and under certain conditions the TDS does not rise to a maximum at all so that $\alpha$ is then zero.

The sharp distinction between cases (*a*) and (*b*) has been confirmed experimentally using the neutron Laue technique on single-crystal silicon (Willis, Carlile & Ward, 1986).

#### 7.4.2.4. *Correction factor for powders*

Thermal diffuse scattering in X-ray powder-diffraction patterns produces a non-uniform background that peaks sharply at the positions of the Bragg reflections, as in the single-crystal case (see Fig. 7.4.2.4). For a given value of the scattering vector, the one-phonon TDS is contributed by all those wavevectors **q** joining the reciprocal-lattice point and any point on the surface of a sphere of radius $2\sin\theta/\lambda$ with its centre at the origin of reciprocal space. These **q** vectors reach the boundary of the Brillouin zone and are not restricted to those in the neighbourhood of the reciprocal-lattice point. To calculate $\alpha$ properly, we require a knowledge, therefore, of the lattice dynamics of the crystal and not just its elastic properties. This is one reason why relatively little progress has been made in calculating the X-ray correction factor for powders.

## 7.4.3. Compton scattering
## (By N. G. Alexandropoulos and M. J. Cooper)

#### 7.4.3.1. *Introduction*

In many diffraction studies, it is necessary to correct the intensities of the Bragg peaks for a variety of inelastic scattering processes. Compton scattering is only one of the incoherent processes although the term is often used loosely to include plasmon, Raman, and resonant Raman scattering, all of which may occur in addition to the more familiar fluorescence radiation and thermal diffuse scattering. The various interactions are summarized schematically in Fig. 7.4.3.1, where the dominance of each interaction is characterized by the energy and momentum transfer and the relevant binding energy.

With the exception of thermal diffuse scattering, which is known to peak at the reciprocal-lattice points, the incoherent background varies smoothly through reciprocal space. It can be removed with a linear interpolation under the sharp Bragg peaks and without any energy analysis. On the other hand, in non-crystalline material, the elastic scattering is also diffused throughout reciprocal space; the point-by-point correction is consequently larger and without energy analysis it cannot be made empirically; it must be calculated. These calculations are imprecise except in the situations where Compton scattering is the dominant process. For this to be the case, there must be an encounter, conserving energy and momentum, between the incoming photon and an individual target electron. This in turn will occur if the energy lost by the photon, $\Delta E = E_1 - E_1$, clearly exceeds the one-electron binding energy, $E_B$, of the target electron. Eisenberger & Platzman (1970) have shown that this binary encounter model – alternatively known as the impulse approximation – fails as $(E_B/\Delta E)^2$.

Table 7.4.3.1. *The energy transfer, in eV, in the Compton scattering process for selected X-ray energies*

| Scattering angle $\varphi$ (°) | Cr $K\alpha$ 5411 eV | Cu $K\alpha$ 8040 eV | Mo $K\alpha$ 17 443 eV | Ag $K\alpha$ 22 104 eV |
|---|---|---|---|---|
| 0 | 0 | 0 | 0 | 0 |
| 30 | 8 | 17 | 79 | 127 |
| 60 | 29 | 63 | 292 | 467 |
| 90 | 57 | 124 | 575 | 915 |
| 120 | 85 | 185 | 849 | 1344 |
| 150 | 105 | 229 | 1043 | 1648 |
| 180 | 112 | 245 | 1113 | 1757 |

Data calculated from equation (7.4.3.1).

The likelihood of this failure can be predicted from the Compton shift formula, which for scattering through an angle $\varphi$ can be written.

$$\Delta E = E_1 - E_2 = \frac{E_1^2(1-\cos\varphi)}{mc^2[1+(E_1/mc^2)(1-\cos\varphi)]}. \qquad (7.4.3.1)$$

This energy transfer is given as a function of the scattering angle in Table 7.4.3.1 for a set of characteristic X-ray energies; it ranges from a few eV for Cr $K\alpha$ X-radiation at small angles, up to $\sim 2$ keV for backscattered Ag $K\alpha$ X-radiation. Clearly, in the majority of typical experiments Compton scattering will be inhibited from all but the valence electrons.

#### 7.4.3.2. *Non-relativistic calculations of the incoherent scattering cross section*

##### 7.4.3.2.1. *Semi-classical radiation theory*

For weak scattering, treated within the Born approximation, the incoherent scattering cross section, $(\mathrm{d}\sigma/\mathrm{d}\Omega)_{\mathrm{inc}}$, can be factorized as follows:

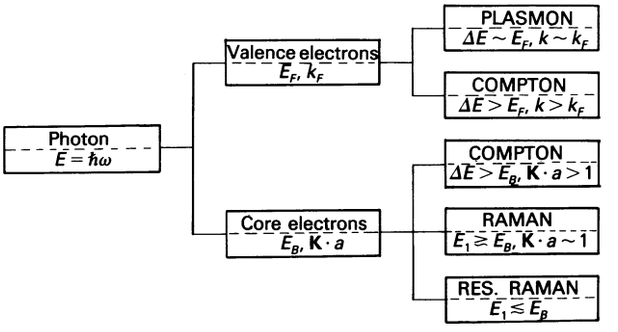


Fig. 7.4.3.1. Schematic diagram of the inelastic scattering interactions, $\Delta E = E_1 - E_2$ is the energy transferred from the photon and **K** the momentum transfer. The valence electrons are characterized by the Fermi energy, $E_F$, and momentum, $k_F$ ($\hbar$ being taken as unity). The core electrons are characterized by their binding energy $E_B$. The dipole approximation is valid when $|\mathbf{K}|a < 1$, where $a$ is the orbital radius of the scattering electron.



references